



HAL
open science

Turbulent flame speed and morphology of pure ammonia flames and blends with methane or hydrogen

Seif Zitouni, Pierre Brequigny, Christine Mouna m-Rousselle

► To cite this version:

Seif Zitouni, Pierre Brequigny, Christine Mouna m-Rousselle. Turbulent flame speed and morphology of pure ammonia flames and blends with methane or hydrogen. Proceedings of the Combustion Institute, In press, 39 (2), pp.2269-2278. 10.1016/j.proci.2022.07.179 . hal-03791714

HAL Id: hal-03791714

<https://hal.science/hal-03791714>

Submitted on 29 Sep 2022

HAL is a multi-disciplinary open access archive for the deposit and dissemination of scientific research documents, whether they are published or not. The documents may come from teaching and research institutions in France or abroad, or from public or private research centers.

L'archive ouverte pluridisciplinaire **HAL**, est destinée au dépôt et à la diffusion de documents scientifiques de niveau recherche, publiés ou non, émanant des établissements d'enseignement et de recherche français ou étrangers, des laboratoires publics ou privés.

Turbulent Flame Speed and Morphology of Pure Ammonia flames and Blends with Methane or Hydrogen

Seif Zitouni^{a,*}, Pierre Brequigny^a, Christine Mounaïm-Rousselle^a

^aUniversity Orléans, PRISME, F-45072 Orléans, France

Abstract

Ammonia appears a promising hydrogen-energy carrier for renewable energy as well as a carbon-free fuel. However, there remain limited studies for ammonia combustion under turbulent conditions. To that end, using the spherically expanding flame configuration, the turbulent flame speeds of stoichiometric ammonia/air, ammonia/methane and ammonia/hydrogen, with mixture composition of blends studied currently being investigated for gas turbine application, were evaluated at various turbulent intensities, covering different kinds of turbulent combustion regimes. Mie-scattering tomography was employed facilitating flame structure diagnosis. Results show that the flame propagation speed of ammonia/air increases exponentially with increasing hydrogen amount, analogous to behavior displayed in the laminar regime. The turbulent to laminar flame speed ratio increases with turbulence intensity, however, smallest gains were observed at the highest hydrogen content, presumably due to differences in the combustion regime, with the mixture located within the flamelet zone, with all other mixtures positioned within the thin reaction zone. A good correlation of the turbulent velocity employing the Karlovitz and Damköhler numbers is observable with the present dataset, as well as previous experimental measurements available in literature, suggesting that ammonia-based fuels may potentially be described following the usual turbulent combustion models. Flame morphology and stretch sensitivity analysis were conducted, revealing that flame curvature remained relatively similar for pure ammonia and ammonia-based mixtures. The wrinkling ratio was found to increase with both increasing ammonia fraction and turbulent intensity, in good agreement with measured increases in turbulent flame speed. On the other hand, in most cases, flame stretch does not change significantly with increasing turbulence, whilst following a similar trend to that of the laminar Markstein length.

Keywords: Ammonia, Turbulent Flame Speed, Turbulent Expanding Flames, Multi-fuel mixtures

*Corresponding author is Seif Zitouni

E-mail: seif-eddine.zitouni@univ-orleans.fr

1. Introduction

Ammonia (NH_3) has been gaining considerable attention over the past decade as a potential zero-carbon alternative fuel to decarbonize our energy systems [1]. However, challenges associated with NH_3 combustion, notably, low flame speed, long ignition delay times, high auto-ignition temperatures and the potential for detrimental emission pollutants (NO_x), have restricted wide-scale application. To minimize or circumvent these issues, oxy-combustion and blending NH_3 with other fuels, such as methane (CH_4) and/or hydrogen (H_2), have been proposed, with successful demonstrations in both gas turbines [2,3] and internal combustion engines [4,5] at high temperature and pressures.

The laminar burning velocity (LBV), a fundamental physiochemical property of a premixed combustible mixture, is a key parameter helping describe premixed operational instabilities, such as flash-back, blow-off or extinction, and an essential step towards characterization of turbulent flame propagation. Recently, experimental research characterizing the LBV of NH_3 based fuels has emerged, including data at high temperatures and pressures. Hayakawa et al. [6] using the spherically expanding flame method, investigated the LBV and Markstein length (L_b) of NH_3/air across a wide range of equivalence ratios (Φ), at 298 K and up to 0.5 MPa. Kanoshima et al., expanded on this work to investigate the influence of temperature up to 500 K [7]. Lhuillier et al. [8] generated an extensive database for NH_3/H_2 mixtures (60 %vol. H_2) at various temperatures (298-473 K), at 0.1 MPa, with Ichikawa et al., investigating H_2/NH_3 (0 to 100%) at 298 K and up to 0.5 MPa [9]. Okafor et al., investigated the influence of CH_4 (53% vol.) upon the LBV of NH_3 flames at 298K and 0.1 MPa [10]. Xia et al. [11] studied the influence of oxygen (O_2) enrichment on NH_3/air flames (O_2 concentration $[\Omega] = 0.35$ & 0.40) for $\Phi = 0.6 - 1.6$, at normal temperature and pressure. In general, the LBV of NH_3 increases linearly with the addition of CH_4 , whilst an exponential increase in LBV of NH_3 is observed with increasing H_2 fraction. An increase in temperature and pressure, produce an inhibiting and enhancing effect, respectively, upon the LBV of NH_3 and its blends with CH_4 and H_2 . Oxygen enhancement of NH_3 flames result in an increase in the LBV, mainly due to the increase in flame temperature without changing the dominant chemistry [11].

Although the research upon the LBV of NH_3 based fuels is widely investigated, there remains limited peer-reviewed studies about turbulence-flame interaction for NH_3 as a fuel, more reflective of practical combustion systems. The turbulent extinction limits of CH_4/NH_3 flames were investigated by Hashimoto et al. [12] with results demonstrating that an increase in CH_4 equated to a widening of NH_3 flammability limit. Ichimura et al., [13] investigated NH_3/air flames at various turbulent

intensities ($u' = 0.32 - 1.61$ m/s). Although the LBV of NH_3/air peaks at $\Phi \sim 1.1$, lean mixtures exhibited better resistance to turbulence induced extinction than at richer conditions, with greater successful propagation over a wider range of Karlovitz numbers (Ka). The authors highlighted the potential thermo-diffusive accelerating effects of lean NH_3/air mixtures, exhibiting Lewis numbers (Le) less than unity. Turbulent CH_4/NH_3 (39 %vol. NH_3) flames have been studied by Ichikawa et al. [14], recording a decreasing turbulent to laminar flame speed ratio (often defined as S_T/S_L^0), with the authors inferring this was mainly explained by a decrease of the flame surface density. Under engine related operating conditions (445K, 0.54 MPa), Lhuillier et al., investigated H_2/NH_3 and CH_4/NH_3 (15% vol. H_2 & CH_4) turbulent flame propagation, also reporting a decreasing S_T/S_L^0 with CH_4 addition, with an increase in S_T/S_L^0 reported for H_2 enrichment, with the authors emphasizing the different thermo-diffusive properties and stretch-related behavior of the fuels [5]. They proposed a correlation, between S_T/S_L^0 and the associated Damköhler (Da) and Ka numbers, showing very good fit with their data, and warranting further investigation. Fan et al. [15], investigated the structures and burning velocities of premixed ammonia/air jet flames at high Ka conditions ($Ka > 100$). They observed a linear increase of S_T/S_L^0 with u'/S_L^0 at high Ka conditions consistent with the thin NH layer observed in their PLIF measurements. Turbulent O_2 -enriched combustion of NH_3 was inspected by Xia et al. [11] ($\Omega = 0.40$), from lean to rich conditions ($\Phi = 0.6 - 1.6$) at various turbulent intensities ($u' = 0.32 - 1.29$ m/s). It was reported that at constant Ka , lean flames displayed a higher turbulent flame speed to unstretched laminar burning velocity ratio than in rich cases, owing to thermo-diffusive properties. Wang et al. [16] investigated the influence of O_2 enrichment ($\Omega = 0.25 - 0.40$) upon NH_3 flames at elevated pressures (0.1-0.3 MPa) and various turbulent intensities ($u' = 0.78 - 2.34$ m/s). The authors concluded that the normalized turbulent flame speed decreases with increasing oxygen content mainly owing to S_L^0 increasing rather than S_T .

The main objectives of this study are: (1) Complete the experimental available database of turbulent flame speed of stoichiometric CH_4/NH_3 and H_2/NH_3 , with mixture composition of blends which are currently being investigated for gas turbine application, whilst also covering different kinds of turbulent combustion regimes. To the author's knowledge, this would represent the first Mie-Scattering tomography study of such NH_3 -based blends, facilitating access to flame structure diagnosis; (2) Validate and improve literature proposed correlations; (3) Examine stretch sensitivity and flame wrinkling of investigated flames.

2. Experimental and Numerical Methods

2.1 Selection of Ammonia-based blends

The mole fraction of CH₄ in NH₃ was varied as 30%, 60% and 100%, with that of H₂ in NH₃ varied as 10%, 30%, 60%. a 90-10% NH₃/H₂ (vol.%) blend was evaluated since it was previously noted by several co-authors in this study to be close to the H₂ addition at which the Lewis number (Le) stopped correlating with S_T/S_L^0 , experimentally [5] and numerically [17]. A 70/30% NH₃/H₂ mixture was investigated as it has demonstrated favorable stability in a generic swirl burner [18], whilst a blend of 40-60% NH₃/H₂ would fall within a different combustion regime to other blends (see Section 3.1), with corresponding 30% and 60% addition of CH₄ to NH₃ evaluated for comparison purposes, as well as 100% CH₄.

Whether in laminar or turbulent configuration all experiments were conducted at stoichiometric conditions ($\Phi = 1.0$), with 3-5 nominally identical experiments for each condition.

2.2 Laminar flame set-up and conditions

Laminar flame speed measurements were performed using a constant-volume spherical vessel. Details of the set-up and post-processing technique can be found in [19] updated with NH₃ specifications in [8]. Measurements for the mixtures were performed at initial conditions of 298K (± 3 K) and 0.1 MPa ($\pm 1 \times 10^{-3}$ MPa). The quasi-steady non-linear association between the stretched-flame speed and stretch was employed [20] - rearranged with the error used for least square regression - to obtain an extrapolated unstretched flame speed and corresponding Markstein Length (L_b). The adiabatic expansion at constant pressure (defined as the ratio of the burnt (ρ_b) to unburnt gas (ρ_u) densities, $\sigma = \rho_b/\rho_u$) was accounted in order to obtain representative values of laminar flame speed, with average results and properties summarized in Table 1 located in the Supplementary Material (SM).

2.3 Turbulent flame set-up and conditions

The combustion vessel described in Section 2.2, was employed using six four-blade fans, positioned in a regular hexahedral configuration, producing a near-isotropic and homogeneous turbulent region within a radius of 20 mm of the vessel center, fully described in [21]. The non-reacting turbulent flow field within the vessel was characterized employing high-speed particle image velocimetry to verify turbulent parameters, namely the turbulent intensity as the rms of the turbulent fluctuation velocity ($u_{rms}=u'$) and the integral length scale (L_T). Minimal changes in the homogeneity and isotropy ratios of the flow field (acceptable range was set at 0.95 & 1.05, $\pm 5\%$ of ideal case) was observed. It was concluded that u' increased linearly with increasing fan speed (ω), expressed as $u' = Af_0$, where $f_0 = (\omega/60)$ and A is a constant = 0.0098m. Finally, by means of two-point velocity correlation, in the longitudinal and lateral directions,

integral length scale was found to be insensitive to the rotational fans speed (2000 – 15000 rpm), remaining almost constant ($L_T \sim 2.64$ mm), in good agreement with previous work and using the same set-up [21].

Three fan speeds were investigated (3000,4000 & 5000 rpm) corresponding to mean turbulent intensities of $u' = 0.49, 0.65$ & 0.82 m/s, respectively. The unburned gas conditions and gas mixtures were identical to those investigated in laminar experiments. It should be noted that pure NH₃/air was evaluated at 423 K. At 298 K, the NH₃/air flame due to its very low laminar flame speed would be conveyed away from the measurement plane, even at lowest turbulence intensities. Increasing the temperature, and thus flame speed, partially resolved this issue, although important losses in sphericity were observable (see Section 3.3).

Mie-scattering laser tomography was employed, enabling enhanced precision with respect to flame front wrinkling by the turbulence. Details of this optical set-up alongside the employed post-processing techniques can be found in [22] and thus only a brief summary is presented here. A Dual-Hawk HP Nd:YAG laser was utilized to illuminate silicon oil droplets, with flame propagation recorded using a Phantom V1610 high-speed camera perpendicular to the laser sheet, set to capture 10,000 fps and facilitating a spatial resolution of 0.0833 mm per pixel. Flame propagation rates were calculated by edge-detection algorithms written in a bespoke MATLAB script. By assuming a spherical flame, from the binarized flame contour images, the surface equivalent flame radius (R_s) and perimeter (R_p), defined as $R_s = (A/\pi)^{1/2}$ and $R_p = (P/2\pi)$, were A represents the burnt gases area and P the perimeter, were determined. The wrinkling ratio (W) was evaluated to be $W = R_p^2/R_s^2$, as defined in [23]. An equivalent flame propagation velocity with respect to the burnt side was derived as $V_T = (dR_s)/dt$. A global flame stretch (K_{global}) was estimated from the flame contour evolution, using the definition of Williams [24] with $K_{global} = (1/A) \cdot (dA/dt)$. Lastly, the local flame curvature was estimated as follows [25]:

$$h = [x(s)'y(s)'' - y(s)'x(s)''] / [(x(s)^2 + y(s)^2)^{3/2}] \quad (1)$$

where $x(s)$ and $y(s)$ the coordinates on the spline curve and s is the curvilinear coordinate. For positive flame front curvature, the local flame front is convex towards the fresh gases, with negative values to regions convex toward the burnt gases.

3. Results and Discussion

3.1 Turbulent Flame Speeds

All experiments performed under various turbulent conditions are shown on the Peters-Borghgi diagram, alongside published NH₃-based datasets in Fig. 1.

Most of the present experiments were located within the thin reaction zone (until 60% H₂ vol.), with that mixture situated within the flamelet regime, a

consequence of a much greater LBV. Notworthily, the mixtures investigated cross the Da=1 limit, not often the case in published NH₃-based literature.

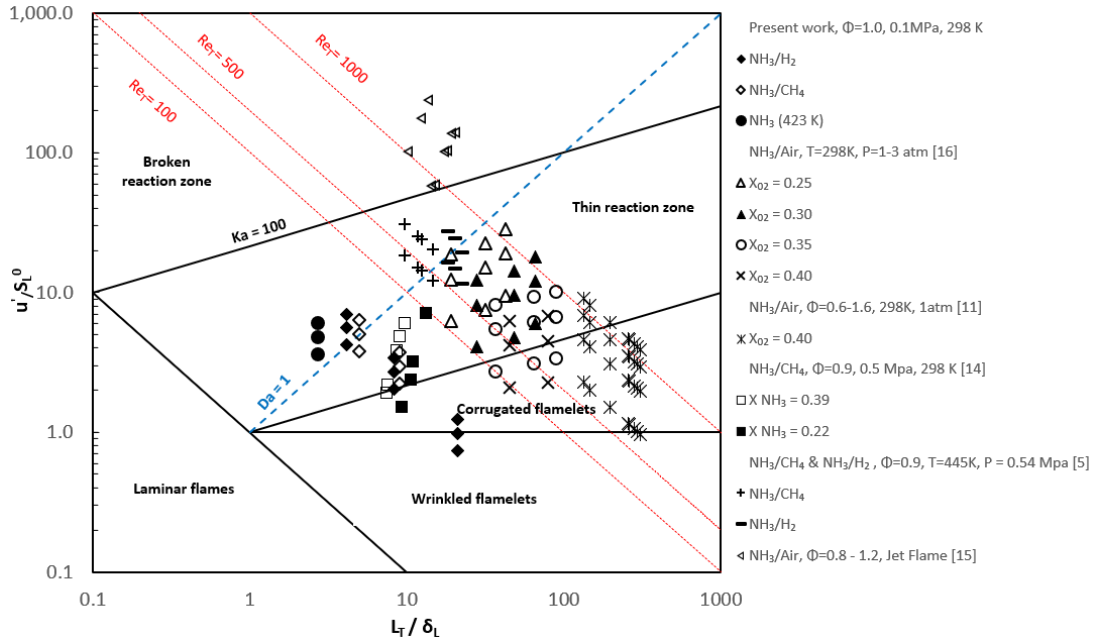


Fig. 1. Present experimental conditions on Peter Borghi [26] diagram alongside literature NH₃-based database

Prior to presenting results, it is worth noting that as reviewed in [27,28], there remains variability and uncertainty in defining basic quantities for the general characterization of turbulent flame propagation as a function of experimental set-ups, measurement techniques and flow conditions. For spherically expanding flames Bradley et al. [29], defined a reference radius (R_v), such that the unburnt gas volume inside a sphere is equal to the burnt gas volume outside it, to estimate the turbulent burning velocity as it would be for a planar flame sheet. This is of importance since for the spherical surface defined by it, the mass turbulent burning velocity and entrainment turbulent burning velocity are equal; with the turbulent flame speed propagation speed equal to the turbulent burning velocity multiplied by the density ratio. The results presented herein were measured using Mie-Scattering tomography, with R_v considered to be equal to the radius obtained from tomographic images R_s , which would equate to a mean progress variable, \tilde{c} , closest to the unburnt side ($\tilde{c} \approx 0.1$), with the evaporation temperature of the Silicon oil droplets ~ 450 K.

As reminded by Lawes et al. [30], the flame can only be wrinkled by smaller sized eddies than its flame front thickness, continually growing until the flame kernel incorporates the entire turbulence spectrum. As such, the flame speed should reach a plateau at some point. Besides, it is of interest to note that even for larger spherical vessels, no experimental

data obtained by [25,31] has reached a clear distinct plateau. As such, there remains no clear consensus concerning the determination of the turbulent burning velocity [32], for spherically expanding flames.

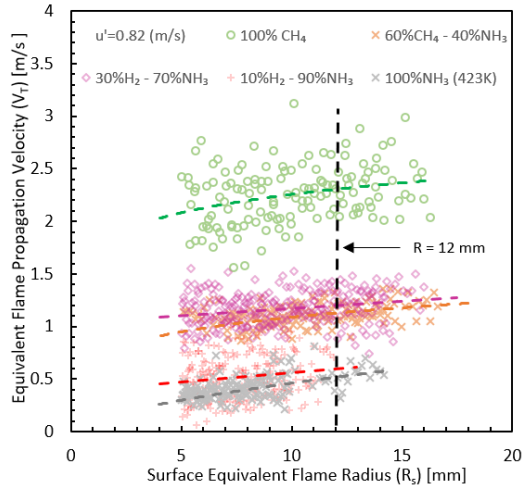


Fig. 2. V_T as a function of flame radius for various blends, $u' = 0.82$ m/s

Commonly, there exists several methods to evaluate S_T , using the raw data of $R(t)$, either using dR/dt (directly taking the time differentiation), or secondly, evaluated as the slope of the best linear fit of $R(t)$ within the experimental domain (equating to an ‘average’ S_T definition). Others, for example

Lawes et al. [30], choose their last measurable data ($R = 30$ mm), whilst Lipatnikov and Chomiak [33] propose that the extrapolation of the evolution of S_T versus the global stretch at zero should provide a more universal value of S_T ($K_{\text{global}} = 0$). Preliminary analysis conducted on our measured S_T values, evaluated the differences between S_T values at $R=12$ mm and S_T ($K_{\text{global}} = 0$) to be $< 20\%$ at highest u' , consistent with the ‘smooth linear profile’ of our raw data, see Fig. 2 and SM (SM 2 and 3).

Due to the homogeneous isotropic turbulent zone in the present experimental set-up, observable flame radii are restricted to 20 mm. As can be seen in Fig. 2 no plateau is identifiable. Moreover, it is worth highlighting that due to the low LBVs of NH_3 -based fuels, some flames were conveyed away from the center of the vessel, by large turbulent structures. As such, the laser sheet did not cut the maximum flame radius, resulting in a limited range of observable radii (see videos in SM). Taking in consideration the above, the mean equivalent propagation velocity (V_T) was evaluated at a constant flame radius, at $R_s=12$ mm.

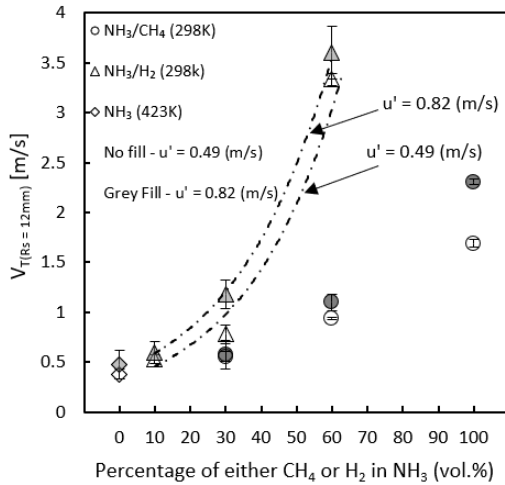


Fig 3. V_T ($R_s=12$ mm) for evaluated blends

Fig. 3 depicts V_T for all the investigated mixtures, at u' of 0.49 and 0.82 m/s. The relatively large scatter is mainly due to the aforementioned loss of sphericity of the flames particularly at highest u' . It is also noted that the NH_3/H_2 blends exhibited greater scatter than the NH_3/CH_4 , particularly at highest u' , potentially due to thermo-diffusional instabilities, although none were observed under laminar conditions. With respect to H_2 addition, irrespective of u' , an exponential increase in V_T is observed, as under laminar conditions (See SM 1). The linear trend upon CH_4 addition to NH_3 under laminar conditions (see SM 1) is less distinguishable under turbulent conditions, particularly at highest u' values.

The turbulent propagation velocity V_T ($R_s=12$ mm) is multiplied by the expansion ratio (ρ_b/ρ_u) to represent a turbulent flame speed (S_T), in an attempt to be

consistent with turbulent correlations based on the ratio S_T/S_L^0 , as in [34]. Fig. 4 presents the evolution of all experimental values of $(\rho_b/\rho_u)(V_T(R_s=12\text{mm})/S_L^0)$ as a function of u'/S_L^0 . It should be underlined that uncertainty bars were omitted for $u'=0.65$ m/s in order to promote graphical clarity. It ought be noted that all S_T/S_L^0 ratio exhibits values < 1 . This may be explained by several reasons (1) the flame is still accelerating at $R_s=12$ mm having not yet reached a plateau since it has not yet been affected by the whole turbulent spectrum as aforementioned (2) the flame is still significantly affected by global stretch which gradually decreases with increasing radius (3) in comparison to Schlieren which projects the whole 3D flame upon a 2D plan leading to a potential flame speed overestimation, Mie-Scattering tomography is a 2D cut of the flame which might not be located at the maximum flame surface area due to the flame conveying, thus potentially leading to an underestimation of flame speed.

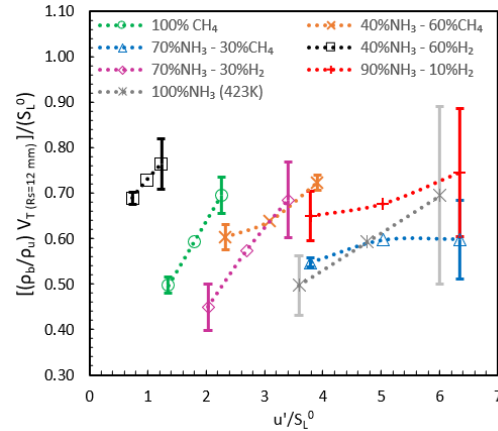


Fig. 4. The variation of $(\rho_b/\rho_u)V_T$ ($R_s=12$ mm)/ S_L^0 as a function of u'/S_L^0 for all conditions

Predictably, an increase in turbulence intensity yields higher $(\rho_b/\rho_u)(V_T(R_s=12\text{mm})/S_L^0)$ ratios for all cases, although only a nominal increase was noted for NH_3/CH_4 (70-30 %vol) between $u' = 0.65$ and 0.82 m/s, however with more important associated uncertainties. Moreover, the smallest gain in S_T/S_L^0 with increasing u' was recorded for the NH_3/H_2 (40-60%), in spite of exhibiting close to double the LBV than any other mixture studied, coupled with the lowest Le ($Le_{\text{eff}} = 0.80$, see SM Table 1). This is presumably due to differences in the combustion regime, with the mixture located within the flamelet zone, with all other mixtures positioned within the thin reaction zone. It is worth underlining that the largest uncertainties are for the pure NH_3 (423 K), NH_3/H_2 (90-10%) and NH_3/CH_4 (70-30%) blends, due to their slow LBVs (0.137, 0.117, 0.129 m/s, respectively), and as a consequence a clear loss of sphericity was observable (see SM 4), presumably due to large turbulent structures interacting with the flame

front. Albeit at a higher unburnt temperature, the pure NH_3 flame exhibits a greater increase in S_T/S_L^0 ratio than the 10% H_2 and 30% CH_4 – NH_3 based flames, although all mixtures display near identical thermo-diffusive and stretched-related properties (L_b [mm] = 1.369, 1.138, 1.079; $Le = 0.96, 0.94, 0.97$, for $\text{NH}_3, \text{H}_2, \text{CH}_4$, respectively).

3.2 Turbulent flame speed correlation

Considering that the mixtures investigated in this study range across two different combustion regimes, with those regimes delimited by characteristic numbers which strongly influence flame propagation behaviour, it seems of interest to compare a literature proposed correlation that incorporate the various turbulent and chemical scales. Lhuillier et al. [5] in their investigation on lean ($\Phi=0.9$) turbulent NH_3/CH_4 and NH_3/H_2 (15 vol%) flames at engine related conditions suggested a correlation based upon a Damköhler (Da) corrected S_T/S_L^0 ratio against the Karlovitz number ($Ka = (u'/S_L^0)^{3/2} / (L_T/\delta_L)^{1/2}$) as:

$$\rho_u/\rho_b (V_T)/S_L^0 = A Da Ka^B \quad (2)$$

with $A = 0.1843$ and $B = 1.1694$

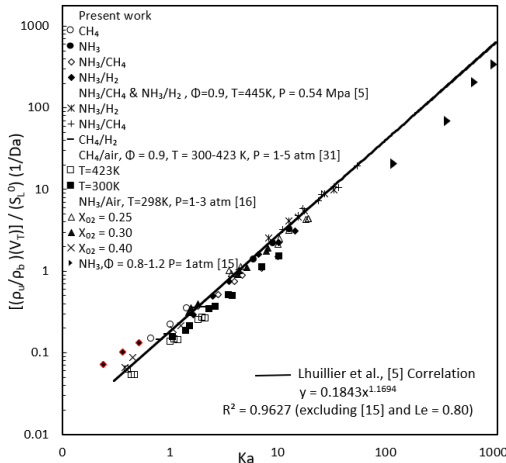


Fig. 5. Correlation of Da -corrected S_T/S_L^0 ratio against Ka . Literature data from expanding flames of Lhuillier et al. [5], Jiang et al. [31], Wang et al. [16] and jet flame of Fan et al. [15].

Fig. 5 illustrates this correlation against various fuel blends, including NH_3 based blends enriched with up to 60% CH_4 and H_2 from this work, oxygen enriched NH_3 ($\Omega=0.25$ - 0.40) [16] and pure CH_4 [31] across a range of temperatures and pressures. A good correlation is observable with the present dataset as well as previous experimental measurements [5] and collapse all available data into the empirical formulation. Furthermore, when all datasets are included, the pre-factor and power exponents of the correlation are very close. It should also be underlined that Wang et al. [16] in their study on oxygen-

enriched NH_3 , proposed a similar correlation that exhibited good correlation to the literature data sets used in Fig. 5. However, we hasten to note that the present correlation seems to be valid only for fuel blends exhibiting near unity Le , since, including the 60% H_2 – 40% NH_3 dataset (\blacklozenge symbol with red outline in left bottom side of Fig. 5), meaningfully reduces both constants and the fitting curves. Additionally, it was deemed of interest to validate experimental data at much higher Ka conditions ($Ka > 100$, broken reaction regime limit), since turbulent NH_3 premixed flames can exhibit much higher turbulence Ka , due to its relative chemical time scale properties (δ_L/S_L^0) in comparison to hydrocarbons [1]. Fan et al. [15] experimental data of premixed ammonia/air jet flames at high Ka showed a relatively satisfactory agreement with Eqn. 2. As such, it is interesting to note that Eqn. 2, yields good agreement with other flame configurations, as highlighted in Lorenzo et al. [34] for gasoline surrogates and methane.

3.3 Morphology and Stretch Analysis

Fig. 6 (a) and (b) show the superimposition of the flame contours centered at regular time intervals for pure NH_3 /air flame at $u' = 0.49$ and 0.82 m/s, respectively. A clear loss of sphericity is observable, presumably due to large turbulent structures interacting with the flame front, most pronounced for mixtures exhibiting lowest flame speeds. It was noted that after the initial ignition energy effects dissipated, lowest-LBV flames would often develop elongated ‘tube or strip’ shapes, similar to the flame structure in the bottom right corner of Fig. 6 (b), in agreement with flame morphologies described by Lhuillier et al. [5]. The averaged wrinkling flame ratio ($W = R_p^2/R_s^2$) against the flame radius is plotted at $u' = 0.49$ and 0.82 m/s, in Fig. 6 (c) and (d), respectively. Results suggest that at lowest turbulence intensity, all blends exhibit similar values, alluding to flame contours displaying similar structure size. As the turbulence increases, all blends exhibit a sharper increase in wrinkling ratio, as expected, since as reminded by Brequigny et al. [22] an increase in u' equates to decreasing the smallest turbulence scales (Kolmogorov and Taylor), consequently enhancing wrinkling. Furthermore, as highlighted in [28], the squared turbulent flame brush thickness (δ_T^2) can be assumed proportional to the product of the turbulent diffusivity and time (t) so that $\delta_T = (u' L_T)^{1/2} \cdot t^{1/2}$, with t measured from the ignition event. The turbulent flame brush will thus increase with u' and time (or radius), enhancing wrinkling and then increasing the flame speed. This appears to corroborate with the flame wrinkling evolution, and the equivalent flame velocity propagation (Fig. 3). Nevertheless, the pure NH_3 /air and the blends with only 10% H_2 and 30% CH_4 displayed a much greater increase in wrinkling flame ratio, with this wrinkling intensification decreasing with higher CH_4 and H_2 content. In an attempt to better understand this intensified wrinkling,

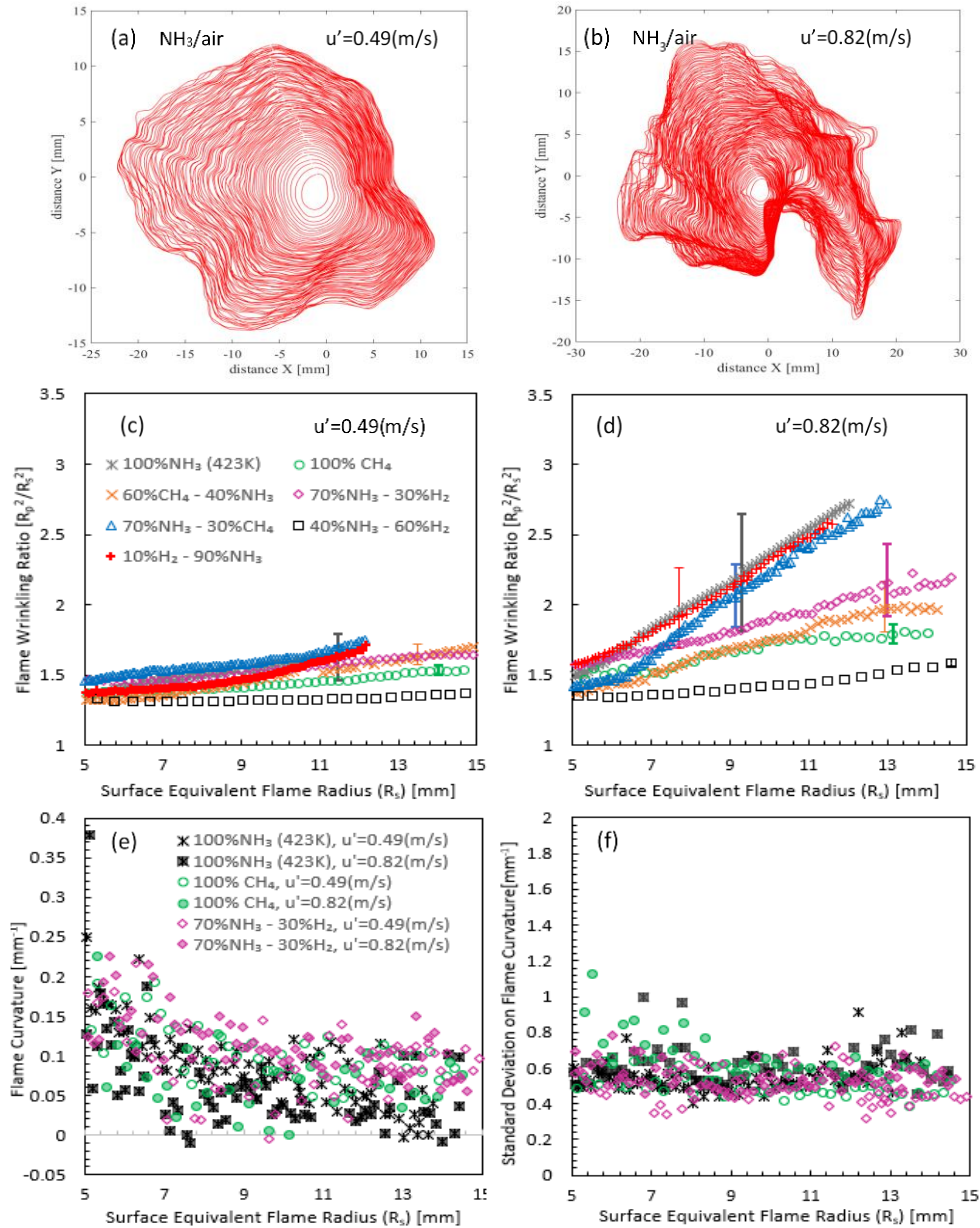


Fig. 6. (a)(b) Flame contour of NH₃/air flame (423 K) for (a) $u'=0.49$ (b) $u'=0.82$ ms⁻¹; (c)(d) Flame wrinkling ratio as a function of flame radius for (c) $u'=0.49$ ms⁻¹ (d) $u'=0.82$ ms⁻¹; (e)(f) Averaged value and standard deviation evolution of the flame curvature, for 100% NH₃, 70%NH₃/30%H₂ and 100% CH₄ at $u'=0.49$ and 0.82 m/s

a mean flame curvature was evaluated by averaging the local value along the flame contour of each image. To enhance clarity, only results for pure NH₃, NH₃/H₂ (70-30%) and pure CH₄ are plotted in Fig. 6(e) and (f) for both u' , since the blends respectively demonstrated high, moderate and low wrinkling ratios respectively as illustrated in Fig. 6 (c) and (d). The full datasets for every dataset are in the SM (SM 5). As can be seen in Fig.6(e), the mean flame curvature decreases from positive to approaching an asymptotic

value close to zero with time according to a hyperbolic evolution. This behavior is maintained irrespective of mixture composition or u' , signifying that initially, the proportion of convex flame front toward the unburnt side is positive, in agreement with the quasi-circular shape of the initial flame kernel. As the flame grows, the ratio of convex to concave flamelet balances. It is noted that all investigated blends exhibit a similar dispersion level with respect to average curvature and standard deviation (Fig. 6

(f), irrespective of the investigated u' , which would tend to suggest similar wrinkling instabilities. Furthermore, all cases illustrated in Fig. 6 (c) and (d) are free of potential Darrieus-Landau instabilities, since for all laminar cases no cellular growth was observed under identical experimental conditions, as well as being thermo-diffusional stable, with Le values close to 1.

In spherically expanding turbulent flames, the flame front is affected not only by local stretch rates related to the wrinkling of the flame front due to the turbulent scales, but as in the laminar case, by the mean global stretch rate [27,29]. In order to compare flame-stretch sensitivity at various turbulence intensities, a global flame stretch (K_{global}) along the flame surface area A is determined from the flame contour evolution. Fig. 7 illustrates the propagation flame speed evolution as a function of K_{global} at $u' = 0.49$ and 0.82 m/s. The tendency curves plotted can be linearly interpolated to evaluate a non-stretched turbulent flame speed, with the stretch sensitivity corresponding to the slope of the extrapolation line.

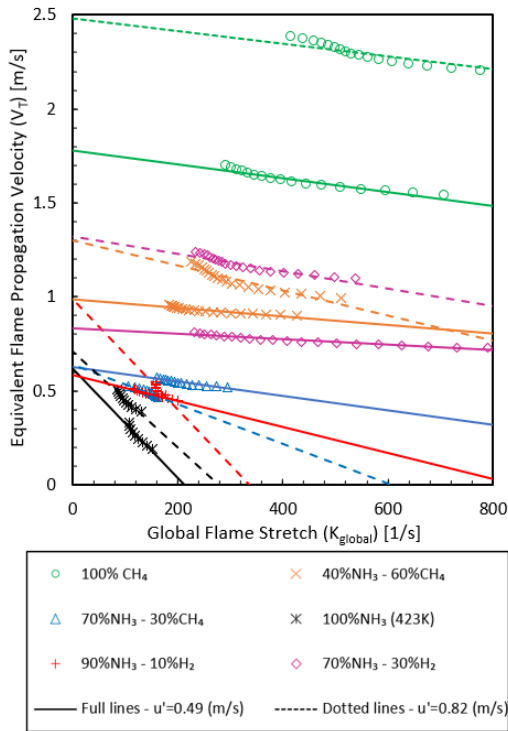


Fig. 7. Equivalent flame speed velocity evolution as a function of global stretch (K_{global})

As can be seen from Fig.7, the flame speed increases with decreasing stretch (i.e. increasing radius) as implied by the positive Markstein length of all mixtures and the increasing wrinkling during the propagation. As expected, for a fixed blend composition, an increase in turbulent intensity results in an increase in the flame speed in agreement with

the increase in flame wrinkling (Fig.6 (c-d)). Flame stretch sensitivity stays relatively constant, or slightly increases in all cases aside from the NH_3-CH_4 (70-30%) mixture, exhibiting a decrease in stretch sensitivity. Nonetheless, in general the stretch sensitivities follow the same ranking as their corresponding laminar Markstein length, in good agreement with previous work [22]. Potentially this behavior could also be due to a decreasing flame thickness, with decreasing NH_3 content.

4. Conclusions

Only a few limited experimental datasets for NH_3 combustion under turbulent conditions are available in literature. To improve the knowledge gap related to the understanding of turbulent-flame interaction of ammonia-based fuels, a first attempt of flame structure study using Mie-Scattering tomography was undertaken. Using the expanding spherical flame configuration, the turbulent flame speed of NH_3 and ammonia blend with up to 60% volume of CH_4 and H_2 were evaluated at various turbulence intensities. Present experimental data, alongside previous literature datasets, including oxygen-enriched NH_3 show good correlation with parameters characteristic of premixed turbulent combustion, Da and Ka . Flame morphology and stretch sensitivity analysis were conducted, revealing that the flame curvature remains relatively similar between NH_3 and other mixtures investigated, following a classical evolution. The wrinkling ratio increases strongly with increasing NH_3 content, a consequence of slower laminar burning velocity and increasing Markstein length. Flame stretch sensitivity does not change significantly with turbulence intensity in most cases, following a similar trend to that of the laminar Markstein length.

Declaration of Competing Interest

The authors declare that they have no known competing financial interest or personal relationships that could have appeared to influence the work reported in this paper.

Acknowledgments

This project has received funding from the European Union's Horizon 2020 research and innovation programme agreement No. 884157.

Supplementary Material

Supplementary Material is available with this work.

References

- [1] H. Kobayashi, A. Hayakawa, K.D.K.A. Somaratne, E.C. Okafor, Science and technology of ammonia combustion, *Proc. Combust. Inst.* 37 (2019) 109–133.
- [2] N.A. Hussein, A. Valera-Medina, A.S. Alsaegh, Ammonia-hydrogen combustion in a swirl burner with reduction of NO_x emissions, *Energy Procedia*, 158 (2019) 2305–2310.

- [3] A. Hayakawa, et al., Experimental investigation of stabilization and emission characteristics of ammonia/air premixed flames in a swirl combustor, *Int. J. Hydrog. Energ.* 42 (2017) 14010–14018.
- [4] C. Lhuillier, P. Brequigny, F. Contino, C. Mounaïm-Rousselle, Experimental study on ammonia/hydrogen/air combustion in spark ignition engine conditions, *Fuel* 269 (2020) 117448.
- [5] C. Lhuillier, P. Brequigny, F. Contino, C. Mounaïm-Rousselle, Experimental investigation on ammonia combustion behavior in a spark-ignition engine by means of laminar and turbulent expanding flames, *Proc. Combust. Inst.*, 38 (2021) 6671–6678.
- [6] A. Hayakawa, et al., Laminar burning velocity and Markstein length of ammonia/air premixed flames at various pressures, *Fuel* 159 (2015) 98–106.
- [7] R. Kanoshima, et al., Effects of initial mixture temperature and pressure on laminar burning velocity and Markstein length of ammonia/air premixed laminar flames, *Fuel* 310 (2022) 122149.
- [8] C. Lhuillier, P. Brequigny, N. Lamoureux, F. Contino, C. Mounaïm-Rousselle, Experimental investigation on laminar burning velocities of ammonia/hydrogen/air mixtures at elevated temperatures, *Fuel* 263 (2020) 116653.
- [9] A. Ichikawa, et al., Laminar burning velocity and Markstein length of ammonia/hydrogen/air premixed flames at elevated pressures, *Int. J. Hydrog. Energ.* 40 (2015) 9570–9578.
- [10] E.C. Okafor, et al., Experimental and numerical study of the laminar burning velocity of CH₄–NH₃–air premixed flames, *Combust. Flame* 187 (2018) 185–198.
- [11] Y. Xia, et al., Turbulent burning velocity of ammonia/oxygen/nitrogen premixed flame in O₂-enriched air condition, *Fuel* 268 (2020) 117383.
- [12] G. Hashimoto, et al., Turbulent flame propagation limits of ammonia/methane/air premixed mixture in a constant volume vessel, *Proc. Combust. Inst.* (2021) 5181–5190.
- [13] R. Ichimura, et al., Extinction limits of an ammonia/air flame propagating in a turbulent field, *Fuel* 246 (2019) 178–186.
- [14] A. Ichikawa, Y. Naito, A. Hayakawa, T. Kudo, H. Kobayashi, Burning velocity and flame structure of CH₄/NH₃/air turbulent premixed flames at high pressure, *Int. J. Hydrog. Energ.* 44 (2019) 6991–6999.
- [15] Q. Fan, et al., Flame structure and burning velocity of ammonia/air turbulent premixed flames at high Karlovitz number conditions, *Combust. Flame* 238 (2022) 111943.
- [16] S. Wang, A.M. Elbaz, Z. Wang, W.L. Roberts, The effect of oxygen content on the turbulent flame speed of ammonia/oxygen/nitrogen expanding flames under elevated pressures, *Combust. Flame* 232 (2021) 111521.
- [17] W. Yang, K.K.J. Ranga Dinesh, K.H. Luo, D. Thevenin, Direct numerical simulation of turbulent premixed ammonia and ammonia-hydrogen combustion under engine-relevant conditions, *Int. J. Hydrog. Energ.* 47 (2022) 11083–11100.
- [18] D. Pugh, et al., Influence of steam addition and elevated ambient conditions on NO_x reduction in a staged premixed swirling NH₃/H₂ flame, *Proc. Combust. Inst.* 37 (2019) 5401–5409.
- [19] B. Galmiche, F. Halter, F. Foucher, Effects of high pressure, high temperature and dilution on laminar burning velocities and Markstein lengths of iso-octane/air mixtures, *Combust. Flame* 159 (2012) 3286–3299.
- [20] A.P. Kelley, C.K. Law, Nonlinear effects in the extraction of laminar flame speeds from expanding spherical flames, *Combust. Flame* 156 (2009) 1844–1851.
- [21] B. Galmiche, N. Mazellier, F. Halter, F. Foucher, Turbulence characterization of a high-pressure high-temperature fan-stirred combustion vessel using LDV, PIV and TR-PIV measurements, *Exp. Fluids* 55 (2014).
- [22] P. Brequigny, F. Halter, C. Mounaïm-Rousselle, Lewis number and Markstein length effects on turbulent expanding flames in a spherical vessel, *Exp. Therm. Fluid Sci.* 73 (2016) 33–41.
- [23] B. Renou, A. Boukhalfá, D. Puechberty, M. Trinité, Effects of stretch on the local structure of freely propagating premixed low-turbulent flames with various Lewis numbers, *Proc. Combust. Inst.* 27 (1998) 841–847.
- [24] A.P. Kelley, A.J. Smallbone, D.L. Zhu, C.K. Law, Laminar flame speeds of C₅ to C₈ n-alkanes at elevated pressures: Experimental determination, fuel similarity, and stretch sensitivity, *Proc. Combust. Inst.* 33 (2011) 963–970.
- [25] D. Bradley, M. Lawes, K. Liu, M.S. Mansour, Measurements and correlations of turbulent burning velocities over wide ranges of fuels and elevated pressures, *Proc. Combust. Inst.* 34 (2013) 1519–1526.
- [26] N. Peters, Turbulent Combustion, *Meas. Sci. Technol.* 12 (2001) 2022.
- [27] A.N. Lipatnikov, J. Chomiak, Turbulent flame speed and thickness: Phenomenology, evaluation, and application in multi-dimensional simulations, *Prog. Energy Combust. Sci.* 28 (2002) 1–74.
- [28] J.F. Driscoll, Turbulent premixed combustion: Flamelet structure and its effect on turbulent burning velocities, *Prog. Energy Combust. Sci.* 34 (2008) 91–134.
- [29] D. Bradley, et al., Turbulent burning velocity, burned gas distribution, and associated flame surface definition, *Combust. Flame* 133 (2003) 415–430.
- [30] M. Lawes, M.P. Ormsby, C.G.W. Sheppard, R. Woolley, The turbulent burning velocity of iso-octane/air mixtures, *Combust. Flame* 159 (2012) 1949–1959.
- [31] L.J. Jiang, S.S. Shy, W.Y. Li, H.M. Huang, M.T. Nguyen, High-temperature, high-pressure burning velocities of expanding turbulent premixed flames and their comparison with Bunsen-type flames, *Combust. Flame* 172 (2016) 173–182.
- [32] P. Brequigny, C. Endouard, F. Foucher, C. Mounaïm-Rousselle, Improvement of Turbulent Burning Velocity Measurements by Schlieren Technique, for High Pressure Isooctane-Air Premixed Flames, *Combust. Sci. Technol.* 192 (2020) 416–432.
- [33] A. Lipatnikov, J. Chomiak, Global stretch effects in premixed turbulent combustion, *Proc. Combust. Inst.* 31 I (2007) 1361–1368.
- [34] M. Di Lorenzo, P. Brequigny, F. Foucher, C. Mounaïm-Rousselle, Turbulent Flame Speed of a Gasoline surrogate in conditions representative of modern downsized Spark-Ignition engine, *Combust. Flame* 240 (2022) 112041.